Measurement-based quantum Otto engine with a two-spin system coupled by anisotropic interaction: Enhanced efficiency at finite times

Chayan Purkait* and Asoka Biswas
Department of Physics, Indian Institute of Technology Ropar, Rupnagar, Punjab 140001, India

(Received 19 December 2022; accepted 14 April 2023; published 8 May 2023)

We have studied the performance of a measurement-based quantum Otto engine (QOE) in a working system of two spins coupled by Heisenberg anisotropic interaction. A nonselective quantum measurement fuels the engine. We have calculated thermodynamic quantities of the cycle in terms of the transition probabilities between the instantaneous energy eigenstates, and also between the instantaneous energy eigenstates and the basis states of the measurement, when the unitary stages of the cycle operate for a finite time τ. The efficiency attains a large value in the limit of $\tau \to 0$ and then gradually reaches the adiabatic value in a long-time limit $\tau \to \infty$. For finite values of τ and for anisotropic interaction, an oscillatory behavior of the efficiency of the engine is observed. This oscillation can be interpreted in terms of interference between the relevant transition amplitudes in the unitary stages of the engine cycle. Therefore, for a suitable choice of timing of the unitary processes in the short time regime, the engine can have a higher work output and less heat absorption, such that it works more efficiently than a quasistatic engine. In the case of an always-on heat bath, in a very short time, the bath has a negligible effect on its performance.

DOI: 10.1103/PhysRevE.107.054110

I. INTRODUCTION

The laws of classical thermodynamics are known to be applicable to the thermodynamic limit. It is quite interesting to study whether these laws are also valid in the quantum limit. In this regard, thermal machines (e.g., heat engines and refrigerators) can be considered as a suitable platform to explore this issue in quantum systems. Deviations from the classical limit of efficiency of these machines can be an important marker to understand the effect of quantum mechanical properties of the system.

In fact, it is rather crucial to explore whether it is possible to enhance the efficiency of thermal machines by harnessing quantum features such as coherence, many-body correlations, and nonthermal population distributions. There have been several studies in different types of quantum heat engine (QHE) models to show that quantum coherence is indeed beneficial to achieve an enhanced performance of the QHEs [1–11]. Roles of quantum correlation and entanglement [12–17], the interaction within a coupled system [18–25], and the nonthermal heat baths [3,26–31] in the performance of quantum thermal machines have been investigated. It was shown that the efficiency of QHEs can be improved beyond the Carnot limit using squeezed thermal baths [27,28,32]. But, their efficiency is bounded by a generalized efficiency limit for QHEs energized by nonthermal heat baths [33].

From the time of Maxwell, it was known that work could be extracted from a single-temperature heat bath using information gained from measurements. This type of engine is known as Szilard's engine, in which results of selective measurement are used to provide feedback on engine operation [34–36]. Recently, it was also shown that projective measurement of the ground state can be used to mimic the release of heat from a system to a cold bath during an isochoric process [37–39] in an ion-based QHE. In later works, quantum measurement has been used to fuel the working system in a QHE, in which the isochoric heating stage in a standard quantum Otto engine (QOE) is replaced by a nonselective quantum measurement [18,24,36,40]. Therefore, the engine works with a single heat bath as a heat shrink and nonselective quantum measurement as a heat source.

A finite-time analysis is also an important aspect of studying QHE; as for practical applications, we need a finite amount of power. Moreover, a QHE in finite time may show true quantum nature in its performance which may not be possible to observe in the quasistatic performance. Standard QHEs are operated by Hamiltonians who do not commute at different times [41–50]. Consequently, quantum internal friction arises when a quantum system is driven unitarily by an external control parameter in finite time. This induces nonadiabatic transitions between the instantaneous eigenstates of the Hamiltonian, and also generates coherence in the energy eigenbasis. As a result, a larger amount of entropy is produced and irreversibility is increased in engine operation, which degrades the performance of QHEs [46–50]. On the other hand, in the presence of quantum coherence, QHEs can produce more power output than the classical ones [7–11,51]. Power output can be improved by not only the finite-time unitary stages, but also via the non-Markovian effects during finite-time bath interaction [52]. In fact, in a very recent study on a finite-time QOE, it has been shown that coherence can act like a dynamical quantum lubricant [45]. This can be interpreted as a dynamical interference effect, which takes place between

*2018phz0001@iitrpr.ac.in

the residual coherence after incomplete thermalization and the coherence generated in the subsequent finite-time unitary driving process.

While the measurement processes and finite-time operation can individually have substantial effects on the performance of the QHEs, there have been very few studies when both protocols are used together. It is recently shown that it is possible to improve the performance of a single-qubit QHE by suitably choosing the measurement basis such that the degradation effect due to coherence production in a standard QOE can be overcome [53]. In this work, we will investigate the finite-time performance of a two-spin QOE by using a nonselective quantum measurement to fuel the engine.

In our model, two spins are coupled with each other by Heisenberg anisotropic XY interaction in the presence of external time-varying homogeneous magnetic fields. By changing the anisotropy parameter one can have the Heisenberg XX or Ising spin Hamiltonian as a limiting case. The free part and the driving part of the Hamiltonian do not commute, leading to the noncommuting nature of the Hamiltonian at two different times. Consequently, it initiates transitions between the instantaneous energy eigenstates, and introduces quantum features into the performance of a QHE through unitary driving processes in finite time. In this paper, we aim to investigate if a measurement-based engine operating in finite time performs better than when operated quasistatically and we show that it is indeed so.

The corresponding enhancement of engine efficiency can be attributed to the anisotropy in the system and the use of the measurement protocol. Such an enhancement could not be achieved if the engine was fueled by a heat bath instead of a nonselective measurement. We will also show that even if the spins remain coupled with a heat bath throughout the cycle (including the stages, when the magnetic fields are varied), it has a negligible effect on the engine's performance for faster unitary stages. However, for a longer duration of these stages, coupling to the bath dominates and the performance of the engine degrades.

The paper is organized as follows. In Sec. II, we introduce the two-spin model of the working system. We describe different stages of the quantum Otto cycle and the relevant thermodynamic quantities. Next in Sec. III, we describe the finite time performance of the cycle. We provide a theoretical analysis of the thermodynamic quantities in terms of the transition probabilities. We also compare them with the quasistatic and the sudden limit of work and efficiency. In Sec. IV, we study the case when the thermal bath continuously interacts with the spins, even when the magnetic field is changed. We conclude the paper in Sec. V.

II. QUANTUM HEAT ENGINE MODEL

In this section, we will briefly introduce our model of the QOE.

A. System model

We consider a system of two spins coupled by Heisenberg anisotropic XY interaction in a transverse magnetic field $[B(t) \geqslant 0]$. The Hamiltonian is represented by [48,54,55]

$$\hat{H(t)} = \hat{H}_0(t) + \hat{H}_I, \tag{1}$$

where

$$\begin{aligned} \hat{H}_0 &= B(t)\left(\hat{\sigma}_1^z + \hat{\sigma}_2^z\right) \\ \hat{H}_I &= J\left[(1+\gamma)\,\hat{\sigma}_1^x\hat{\sigma}_2^x + (1-\gamma)\,\hat{\sigma}_1^y\hat{\sigma}_2^y\right]. \end{aligned} \tag{2}$$

Here $\hat{H}_0$ is the free part of the Hamiltonian, and $\hat{H}_I$ represents the interaction between two spins with $\gamma \in [-1, 1]$ [56,57] as the anisotropy parameter, and J is the coupling constant between the spins. The operators $\hat{\sigma}_i^{x,y,z}$ are the standard Pauli matrices for the ith $(i \in 1, 2)$ spin. If $\gamma = 0$, the Hamiltonian becomes a Heisenberg isotropic XX type, and for $\gamma = \pm 1$, this becomes the Ising spin Hamiltonian. For $\gamma \neq 0$, $\hat{H}_I$ and $\hat{H}_0$ do not commute, which in turn gives rise to $[\hat{H}(t), \hat{H}(t')] \neq 0$. This further indicates that we may see quantum behavior in finite-time engine operation [50].

The eigenvectors and the corresponding eigenvalues of the Hamiltonian $\hat{H}(t)$ are given by

$$\begin{aligned} |\psi_0\rangle &= \frac{1}{\sqrt{2}}\left(\frac{B-K}{\sqrt{K^2-BK}}|11\rangle + \frac{\gamma J}{\sqrt{K^2-BK}}|00\rangle\right), & E_0 &= -2K, \\ |\psi_1\rangle &= \frac{1}{\sqrt{2}}(-|10\rangle + |01\rangle), & E_1 &= -2J, \\ |\psi_2\rangle &= \frac{1}{\sqrt{2}}(|10\rangle + |01\rangle), & E_2 &= 2J, \\ |\psi_3\rangle &= \frac{1}{\sqrt{2}}\left(\frac{B+K}{\sqrt{K^2+BK}}|11\rangle + \frac{\gamma J}{\sqrt{K^2+BK}}|00\rangle\right), & E_3 &= 2K, \end{aligned} \tag{3}$$

where $K = \sqrt{B^2 + \gamma^2 J^2}$. These energy eigenstates can be divided into two categories. The states that are dependent on the system parameters $B(t)$ and J, namely $|\psi_0\rangle$ and $|\psi_3\rangle$, evolve with time. The other ones which are independent of the system parameters, namely $|\psi_1\rangle$ and $|\psi_2\rangle$, are the standard Bell states that remain unchanged with time. We will show in this work that the former ones play a fundamental role in the behavior of the measurement-based cycle. Note that in the limit of $\gamma = 0$, the eigenstates $|\psi_{0,3}\rangle$ take the form of product (i.e., disentangled) states, with the respective eigenvalues $\mp 2B$ [see Appendix A].

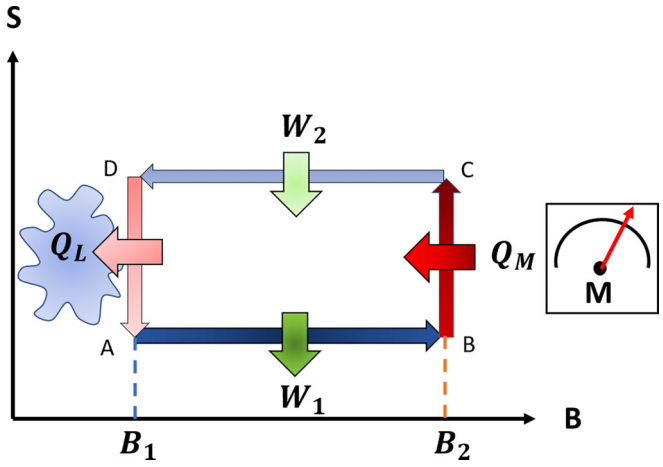

FIG. 1. Schematic diagram of the Otto cycle.

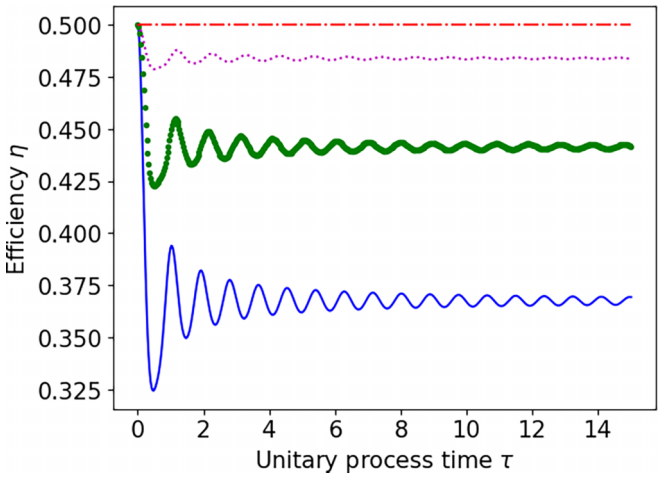

FIG. 2. Efficiency as a function of duration τ of the unitary stages for different values of the anisotropy parameter $\gamma = 0$ (dash dotted red line), $\gamma = 0.3$ (point marked magenta line), $\gamma = 0.6$ (dotted green line), $\gamma = 1$ (solid blue line). The other parameters are $B_1 = 1$, $B_2 = 2$, $T = 1$. All the quantities are dimensionless with respect to J and also we have used $k_B = \hbar = 1$.

B. Quantum Otto cycle and thermodynamic quantities

We consider that the working system undergoes an Otto cycle. The schematic diagram of the cycle is shown in Fig. 1. The stages of the cycle are described below.

Unitary expansion (A to B): The working system is initially prepared in a thermal state $\hat{\rho}_A = e^{-\beta \hat{H}_1}/Z$ at inverse temperature $\beta = 1/T (k_B = 1)$, with $\hat{H}_1 = \hat{H}(0)$ and $Z = \mathrm{Tr}(e^{-\beta \hat{H}_1})$. During this stage of the cycle, the system is decoupled from the heat bath and the external magnetic field is changed from B_1 to B_2 during a finite timeinterval τ. We choose a linear ramp for this change: $B(t) = B_1 + (B_2 - B_1)(t/\tau)$, where $0 \leqslant t \leqslant \tau$. The state of the working system at the end of this stage changes to $\hat{\rho}_B = \hat{U}(\tau)\hat{\rho}_A\hat{U}^\dagger(\tau)$, where $\hat{U}(\tau) = \mathcal{T}\exp[-\iota \int_0^\tau dt \hat{H}(t)]$ is the relevant time evolution operator, with $\mathcal{T}$ indicating the timeordering. Also, a certain amount of work W_1 is done by the system, which can be calculated as $W_1 = \langle E_B\rangle - \langle E_A\rangle$, where $\langle E_A\rangle = \mathrm{Tr}(\hat{\rho}_A\hat{H}_1)$ and $\langle E_B\rangle = \mathrm{Tr}(\hat{\rho}_B\hat{H}_2)$ indicate the expectation values of the internal energies of the system at the start and the end of this stage. Note that $\hat{H}_2 = \hat{H}(\tau)$.

Isochoric heating (B to C): The heating of a system can be generally understood to be associated with an increase in its entropy. Usually, a system is heated using a heat bath. This can be alternatively achieved by applying a nonselective quantum measurement on the working system. In order to ensure that the energy supplied by this measurement is nonzero, the measurement operator $\hat{M}$ should not commute with the Hamiltonian, i.e., $[\hat{H}(B_2), \hat{M}] \neq 0$. If $\hat{\rho}$ is the state before the measurement, the post-measurement state is usually written as $\sum_\alpha \hat{M}_\alpha\hat{\rho}\hat{M}_\alpha$, where $\hat{M}_\alpha = |M_\alpha\rangle\langle M_\alpha|$ is the projection operator associated to the nondegenerate eigenvalues of the observable M with eigenstates $|M_\alpha\rangle$, satisfying $\hat{M}_\alpha^\dagger = \hat{M}_\alpha$ and $\sum_\alpha \hat{M}_\alpha^2 = \mathbb{1}$. In the present case, we perform a global measurement of the state of the system; in the Bell basis $\{|\psi_\pm\rangle = \frac{1}{\sqrt{2}}(|00\rangle \pm |11\rangle), |\phi_\pm\rangle = \frac{1}{\sqrt{2}}(|01\rangle \pm |10\rangle)\}$. The leads to a post-measurement state given by $\hat{\rho}_C = \sum_{\alpha=1}^4 \hat{M}_\alpha\hat{\rho}_B\hat{M}_\alpha$, where $\hat{M}_\alpha$ describes the relevant projection operators as follows: $\hat{M}_{1,2} = |\psi_\pm\rangle\langle\psi_\pm|$ and $\hat{M}_{3,4} = |\phi_\pm\rangle\langle\phi_\pm|$. During this stage, the entropy of the system increases due to its interaction with the measurement apparatus and this increase can be considered equivalent to heating. The corresponding heat "absorbed" can be calculated as $Q_M = \langle E_C\rangle - \langle E_B\rangle$, where the internal energy $\langle E_C\rangle = \mathrm{Tr}(\hat{\rho}_C\hat{H}_2)$.

Unitary compression (C to D): The working system remains decoupled from the heat bath in this stage. The magnetic field is driven from B_2 to B_1 in a finite time τ using the protocol $B(\tau - t)$. The state of the working system at the end of this stage becomes $\hat{\rho}_D = \hat{V}(\tau)\hat{\rho}_C\hat{V}^\dagger(\tau)$, where $\hat{V}(\tau) = \mathcal{T}\exp[-\iota \int_0^\tau dt \hat{H}(\tau - t)]$ is the time evolution operator. A certain amount of work, W_2, is done on the system, which can be calculated as $W_2 = \langle E_D\rangle - \langle E_C\rangle$, where the internal energy $\langle E_D\rangle = \mathrm{Tr}(\hat{\rho}_D\hat{H}_1)$.

Isochoric cooling (D to A): During this final stage of the cycle, the system is now coupled with a heat bath at the temperature T, whereas the magnetic field remains fixed at B_1. The system releases some amount of heat Q_L to the bath, which can be calculated as $Q_L = \langle E_A\rangle - \langle E_D\rangle$. We assume that this process is carried out over a long time so that the system reaches thermal equilibrium with the bath.

Total work done in a complete cycle can be calculated as $W = (W_1 + W_2) = -(Q_M + Q_L)$. If $W < 0$, then the total work in a complete cycle is done by the working system. Also, the working system absorbs some amount of heat in the measurement process, if $Q_M > 0$. Then, the working system in a complete cycle works as a heat engine. So, the efficiency of the engine is given by $\eta = |W|/Q_M$.

III. FINITE TIME OPERATION OF THE ENGINE

Usually, quantum heat engines are studied quasistatically. If we allow different stages of the engine cycle only for finite times, the performance of the engine is expected to deviate substantially from the steady state. We show in Fig. 2 how the efficiency varies with respect to the duration of the unitary stages. We assume that each of these stages (unitary expansion and compression) occurs for the same duration τ. All simulations are done using QuTip [58] software package.

As seen in Fig. 2, the efficiency oscillates at the transient timescale for $\gamma \neq 0$. This means that if the unitary stages are executed for a very short time $\tau \gtrsim 0$, the efficiency can be larger or smaller than that obtained for a large value of τ. If the unitary processes are prolonged, the oscillation in efficiency disappears. Thus, a finite-time measurement-based engine can perform better than the same engine operating for a longer duration for a suitable selection of the duration τ for unitary processes.

Note that, if one would use a local measurement, instead of global ones, similar oscillatory behavior in the efficiency of the engine could be seen for finite-time operation [18,24]. Also in these cases, the engine performs better than its quasistatic counterpart at finite times for specific choices of the local basis.

A. Thermodynamic quantities in terms of transition probabilities

The results as mentioned above can further be analyzed in terms of the transition probabilities between the instantaneous eigenstates of the Hamiltonian. The internal energies (derivations are given in the Appendix B) of the system at four vertices of the QHE diagram in Fig. 1, are given by

$$\begin{aligned}
\langle E_A\rangle &= -4K_1\frac{\sinh 2K_1\beta}{Z} - 4J\frac{\sinh 2J\beta}{Z},\\
\langle E_B\rangle &= -4K_2(1-2\xi)\frac{\sinh 2K_1\beta}{Z} - 4J\frac{\sinh 2J\beta}{Z},\\
\langle E_C\rangle &= -4K_2(1-2\delta)(1-2\chi)\frac{\sinh 2K_1\beta}{Z} - 4J\frac{\sinh 2J\beta}{Z},\\
\langle E_D\rangle &= -4K_1(1-2\delta)(1-2\lambda)\frac{\sinh 2K_1\beta}{Z} - 4J\frac{\sinh 2J\beta}{Z},
\end{aligned} \tag{4}$$

where $Z = 2\cosh(2K_1\beta) + 2\cosh(2J\beta)$ is the partition function, and $K_1 = \sqrt{B_1^2+\gamma^2J^2}$, $K_2 = \sqrt{B_2^2+\gamma^2J^2}$, $\xi = |\langle\psi_0^{(2)}|\hat{U}(\tau)|\psi_3^{(1)}\rangle|^2$, $\delta = |\langle\psi_+|\hat{U}(\tau)|\psi_0^{(1)}\rangle|^2$, $\chi = |\langle\psi_0^{(2)}|\psi_+\rangle|^2$, and $\lambda = |\langle\psi_3^{(1)}|\hat{V}(\tau)|\psi_-\rangle|^2$. Clearly, ξ accounts for the transition probability between two different eigenstates $|\psi_3\rangle$ and $|\psi_0\rangle$ during the unitary expansion. Also, because the instantaneous energy eigenstates $|\psi_{0,3}\rangle$ do not truly coincide with the measurement basis states $|\psi_\pm\rangle$, their nonzero overlap gives rise to certain transitions between them during measurement and unitary compression stages of the cycle. This can be seen by rewriting the states $|\psi_\pm\rangle$ in terms of the instantaneous energy eigenstates as

$$\begin{aligned}
|\psi_+\rangle &= -\frac{c_2-d_2}{a_2d_2-b_2c_2}\big|\psi_0^{(2)}\big\rangle + \frac{a_2-b_2}{a_2d_2-b_2c_2}\big|\psi_3^{(2)}\big\rangle,\\
|\psi_-\rangle &= -\frac{c_2+d_2}{a_2d_2-b_2c_2}\big|\psi_0^{(2)}\big\rangle + \frac{a_2+b_2}{a_2d_2-b_2c_2}\big|\psi_3^{(2)}\big\rangle,
\end{aligned} \tag{5}$$

where

$$\begin{aligned}
a_2 &= \frac{B_2-K_2}{\sqrt{K_2^2-B_2K_2}}, \quad b_2 = \frac{\gamma J}{\sqrt{K_2^2-B_2K_2}},\\
c_2 &= \frac{B_2+K_2}{\sqrt{K_2^2+B_2K_2}}, \quad d_2 = \frac{\gamma J}{\sqrt{K_2^2+B_2K_2}}.
\end{aligned} \tag{6}$$

Then the relevant transition probabilities can be written as

$$\begin{aligned}
\delta &= \Big| -\frac{c_2-d_2}{a_2d_2-b_2c_2}\big\langle\psi_0^{(2)}\big|U(\tau)\big|\psi_0^{(1)}\big\rangle\\
&\quad + \frac{a_2-b_2}{a_2d_2-b_2c_2}\big\langle\psi_3^{(2)}\big|U(\tau)\big|\psi_0^{(1)}\big\rangle\Big|^2,\\
\lambda &= \Big| -\frac{c_2+d_2}{a_2d_2-b_2c_2}\big\langle\psi_3^{(1)}\big|V(\tau)\big|\psi_0^{(2)}\big\rangle\\
&\quad + \frac{a_2+b_2}{a_2d_2-b_2c_2}\big\langle\psi_3^{(1)}\big|V(\tau)\big|\psi_3^{(2)}\big\rangle\Big|^2,
\end{aligned} \tag{7}$$

and

$$\chi = \left|\frac{c_2-d_2}{a_2d_2-b_2c_2}\right|^2. \tag{8}$$

The expressions of the work can be obtained using Eq. (4) as

$$W_1 = 4[K_1 - K_2(1-2\xi)]\frac{\sinh 2K_1\beta}{Z}$$

and

$$W_2 = 4(K_2-K_1)(1-2\delta)(1-2\lambda)\frac{\sinh 2K_1\beta}{Z}.$$

Thus, the total work in a complete cycle is given by

$$\begin{aligned}
W = W_1 + W_2 &= -4[K_2\{(1-2\xi) - (1-2\delta)(1-2\chi)\}\\
&\quad - K_1\{1-(1-2\delta)(1-2\lambda)\}]\frac{\sinh 2K_1\beta}{Z}.
\end{aligned} \tag{9}$$

Also, the heat "absorption" during the measurement stage is given by

$$Q_M = 4K_2[(1-2\xi) - (1-2\delta)(1-2\chi)]\frac{\sinh 2K_1\beta}{Z}. \tag{10}$$

The efficiency of the cycle is therefore given by

$$\eta = \frac{|W|}{Q_M} = 1 - \frac{K_1[1-(1-2\delta)(1-2\lambda)]}{K_2[(1-2\xi)-(1-2\delta)(1-2\chi)]}. \tag{11}$$

The plot of the transition probabilities ξ, δ, χ, and λ with respect to the duration τ of the individual unitary processes are shown in Fig. 3. Note that δ and λ exhibit oscillatory dependence on τ, χ remains constant, while ξ displays a monotonic decay, as τ increases. Though the transition probabilities δ and λ are the same, for our choice of the measurement basis and the eigenstates of the Hamiltonian, it is, generally speaking, not a universal feature [53].

The oscillation in the finite time efficiency is primarily due to the oscillation in the transition probabilities δ and λ. The oscillation in the transition probabilities δ can be attributed to the interference between the probability amplitudes for the transitions $|\psi_0^{(1)}\rangle \to |\psi_0^{(2)}\rangle$ and $|\psi_0^{(1)}\rangle \to |\psi_3^{(2)}\rangle$ [see Eq. (7)]. Similarly, oscillation in λ is due to the transition $|\psi_-\rangle \leftrightarrow |\psi_3^{(1)}\rangle$. The other transition probability ξ, also known as quantum internal friction [50,59], is negligible with respect to the δ, χ, and λ in a measurement-based QHE. As the unitary stages are prolonged, oscillation in the finite time efficiency disappears and the efficiency approaches to the quasistatic limit (see Sec. III B).

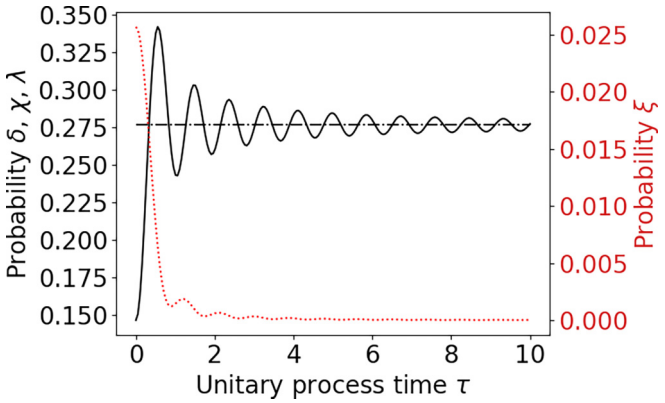

FIG. 3. Transition probabilities as a function of the duration τ of each unitary stage. We have used the left y axis for transition probabilities δ and λ (solid black line), and χ (dash dotted black line) and the right y axis for transition probability ξ (point marked red line). The other parameters are $B_1 = 1$, $B_2 = 2$, and $\gamma = 1$.

Note that the two energy eigenstates $|\psi_1\rangle$ and $|\psi_2\rangle$ are the same as two Bell states $|\phi_\pm\rangle$. As these states have been used in measurement basis, their occupation probabilities do not change in the measurement process, and therefore, these states do not contribute to the calculation of heat [see Eqs. (7), (8), and (10)]. Moreover, the eigenvalues of these eigenstates are independent of the external control parameter $B(t)$, and thus the contribution of these states to work is also zero [see Eq. (9)]. The only contribution to the engine performance arises from the two other eigenstates $|\psi_0\rangle$ and $|\psi_3\rangle$.

B. Quasistatic (adiabatic) limit of the thermodynamic quantities

In order to calculate the quasistatic value of the efficiency, we consider that the unitary processes are performed quasistatically, i.e., for an infinite time interval. Therefore, there are no nonadiabatic transitions between two instantaneous energy eigenstates, and the unitary processes become adiabatic. So, in such a limit, we can write $\xi = |\langle\psi_0^{(2)}|\hat{U}(\tau)|\psi_3^{(1)}\rangle|^2 \overset{\tau\to\infty}{=} 0$ (Fig. 3). Also, the transition probabilities between the instantaneous energy eigenstates and the basis states of measurement take the following forms for very large τ:

$$\delta \overset{\tau\to\infty}{=} \left|\frac{c_2 - d_2}{a_2 d_2 - b_2 c_2}\right|^2, \quad \lambda \overset{\tau\to\infty}{=} \left|\frac{a_2 + b_2}{a_2 d_2 - b_2 c_2}\right|^2.$$

Using the expressions of a_2, b_2, c_2, d_2 [see Eq. (6)] we can indeed find that $\delta = \chi = \lambda = \frac{1}{2} - \gamma J/2K_2$ at the quasistatic limit (see also Fig. 3).

Thus, the expressions of the work and heat absorption of the cycle can be obtained as

$$W_q = -16(K_2 - K_1)\chi(1-\chi)\frac{\sinh 2K_1\beta}{Z},$$
$$Q_{Mq} = 16K_2\chi(1-\chi)\frac{\sinh 2K_1\beta}{Z}, \tag{12}$$

and the quasistatic value of the efficiency is given by

$$\eta_q = |W_q|/Q_{Mq} = 1 - \frac{K_1}{K_2}. \tag{13}$$

Clearly, the expression of this efficiency is independent of the temperature of the heat bath used in the cold isochoric process. This indicates that the performance of the engine does not depend upon the temperature of the heat bath in the case of global measurement, which we have used in the isochoric heating stage. We emphasize that this is unlike the case for a local measurement where the performance of an engine depends upon the temperature of the heat bath [18]. Also, it can be seen from Eq. (13) that for nonzero γ, the expression of the efficiency is very much similar to the efficiency of a single-spin QHE with two heat baths [42] or a single heat bath and a nonselective quantum measurement at the isochoric heating stage [40]. This similarity arises as only two intermediate energy levels ($|\psi_{0,3}\rangle$, as mentioned in Sec. II A) contribute to the engine performance due to our specific choice of the measurement basis. Therefore, a measurement-based heat engine with a coupled two-spin working system for global measurement acts like a two-level (single-spin) heat engine, which is evident in the expression of the efficiency [Eq. (13)]. Interestingly, even a two-stroke QHE made up of two different working systems with two different frequencies can lead to the same form of efficiency [60]. However, the expression of efficiency will differ if one uses a coupled two-spin working system along with two heat baths or with a single bath plus local measurement instead of global measurement.

C. Sudden (quench) limit of the thermodynamic quantities

In order to calculate the sudden limit of the thermodynamic quantities, we consider that the external magnetic field is changed suddenly ($\tau \to 0$) from B_1 to B_2 or vice versa. In this case $\hat{U}(\tau), \hat{V}(\tau) \to \mathbb{1}$, therefore the state of the system does not change over unitary processes. So, in this limit, the transition probabilities can be written as

$$\delta \overset{\tau\to 0}{=} \left|-\frac{c_2 - d_2}{a_2 d_2 - b_2 c_2}\langle\psi_0^{(2)}|\psi_0^{(1)}\rangle + \frac{a_2 - b_2}{a_2 d_2 - b_2 c_2}\langle\psi_3^{(2)}|\psi_0^{(1)}\rangle\right|^2$$
$$= -\frac{(B_1 - K_1 + \gamma J)^2}{4K_1(B_1 - K_1)},$$
$$\lambda \overset{\tau\to 0}{=} \left|-\frac{c_2 + d_2}{a_2 d_2 - b_2 c_2}\langle\psi_3^{(1)}|\psi_0^{(2)}\rangle + \frac{a_2 + b_2}{a_2 d_2 - b_2 c_2}\langle\psi_3^{(1)}|\psi_3^{(2)}\rangle\right|^2$$
$$= \frac{(B_1 + K_1 - \gamma J)^2}{4K_1(B_1 + K_1)},$$
$$\xi \overset{\tau\to 0}{=} |\langle\psi_0^{(2)}|\psi_3^{(1)}\rangle|^2 = -\frac{\gamma^2 J^2 + (B_1 + K_1)(B_2 - K_2)}{4K_1K_2(B_2 - B_1)(B_1 + K_1)}. \tag{14}$$

Also from Eq. (8), we get

$$\chi = \frac{(B_2 - K_2)(B_2 + K_2 - \gamma J)^2}{4\gamma J^2 K_2}. \tag{15}$$

Using (14) and (15) in the expressions of work [Eq. (9)] and heat absorption [Eq. (10)], we obtain the sudden limits of work and heat absorption which are given by

$$W_s = -4\frac{B_1(B_2 - B_1)}{K_1}\frac{\sinh 2K_1\beta}{Z},$$
$$Q_{Ms} = 4\frac{B_1 B_2}{K_1}\frac{\sinh 2K_1\beta}{Z}. \tag{16}$$

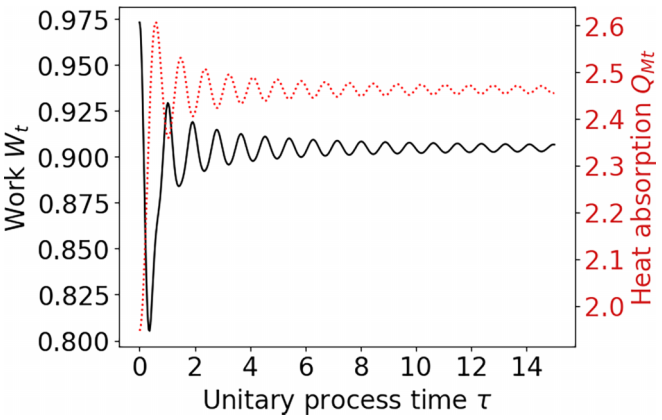

FIG. 4. Variation of the absolute value of the work done W_t (solid black line, labeled on the left y axis) and heat absorbed Q_{Mt} (point marked red line, labeled on the right y axis) as a function of duration τ of the unitary stage. The other parameters are $B_1 = 1$, $B_2 = 2$, $T = 1$, and $\gamma = 1$.

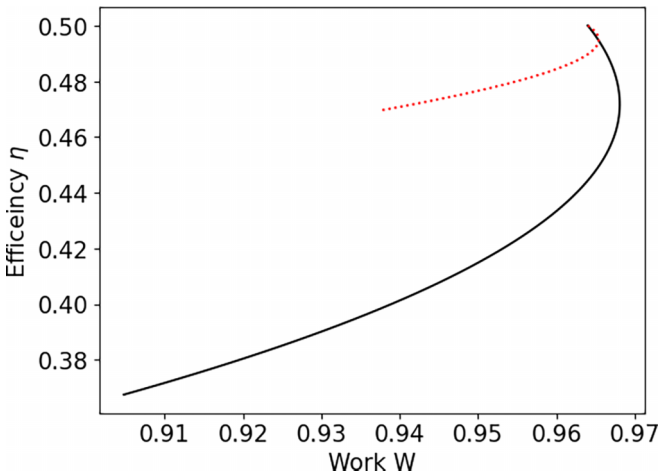

FIG. 5. The parametric plot of the variable γ on the work-efficiency plane. We have taken the absolute value of the work. Here the point-marked red line represents the finite-time value (for $\tau = 0.1$) and the solid black line represents the quasistatic value. The anisotropy parameter γ varies from 0 to 1. The point 0.5 on the solid black line corresponds to $\gamma = 0$, while the left end of the plot corresponds to $\gamma = 1$. The other parameters are $B_1 = 1$, $B_2 = 2$, and $T = 1$.

Therefore, the efficiency at this limit is given by

$$\eta_s = \frac{|W_s|}{Q_{Ms}} = 1 - \frac{B_1}{B_2}. \tag{17}$$

Interestingly, the efficiency does not depend on the anisotropy parameter in the sudden limit. This means that the QOE has the same efficiency for all γ when $\tau \to 0$. This can be seen in Fig. 2 that, for our choices of $B_1 = 1$ and $B_2 = 2$, this is equal to 0.5, irrespective of the values of γ, whereas for large τ, the efficiency saturates to a lower value. Therefore, with two spins coupled by anisotropic interaction as the working system, a measurement-based QHE operating in the sudden limit performs better than an engine operating in the adiabatic limit.

D. Analysis of the heat engine performance

For the quasistatic operation of the cycle, we show the variation of the efficiency as a function of work in Fig. 5. It is clear from this plot that the engine performance degrades with the increase of the anisotropy parameter γ. This is because as γ increases, the heat absorption in the measurement process increases and the work output decreases after a slow increase in the lower range of γ. We also observed that there exists a certain value of $\gamma \sim 0.46$ for which the work output gets maximized.

The variation of the work and heat absorption with respect to the duration τ of the unitary processes are shown in Fig. 4. Also, the plots of the efficiency with respect to work are shown in Fig. 5. From these plots, we can see that a finite-time engine can deliver more work than the same engine operating in the quasistatic limit with a proper choice of the time interval τ of the unitary processes. In addition to that, the finite-time engine absorbs less amount of heat in the measurement process than the same engine operating in the quasistatic limit. Consequently, when operated for finite times, the engine requires less energy resource, and still can perform better than its quasistatic counterpart.

Interestingly, this outperforming is further improved for the larger anisotropy parameter γ. When $\gamma = 0$, no transition takes place between two instantaneous energy eigenstates, and the unitary stages remain adiabatic, irrespective of their duration. Also, there is no interference-like effect between two transition probability amplitudes for the isotropic case [see Appendix A], unlike in the anisotropic case. Thus, the efficiency does not change with respect to τ, as displayed in Fig. 2. Therefore, operating the engine even for a finite time would lead to the same efficiency as for the case when operated quasistatically.

IV. ALWAYS-ON COUPLING TO THE HEAT BATH

It may not always be possible to decouple a quantum system from its bath, which acts as a heat bath for the HE operation, depending upon the architecture of the working system and the bath. Also, there is a cost associated with coupling and decoupling the working system from a heat bath [61,62]. In the previous section, we assumed that the working system is completely isolated from its bath during the work-delivering stages so that the stages, AB and CD, remain unitary. We consider here that the HE operation is implemented in a type of realistic architecture in which the working system cannot be decoupled from its bath [61]. It is therefore necessary to take into account the dissipation of energy from the working system to the bath during stages AB and CD. This requires solving the master equation, which is given below, with a time-dependent Hamiltonian under a dissipative bath. Here, we assume that the remaining two isochoric stages of the cycle are identical to those mentioned in Sec. II B. Furthermore, since the measurement process is assumed to be instantaneous, the bath will not have any effect on the system during measurement.

We consider that the temperature of the heat bath is T and a single spin decays to the bath. Then the master equation in the interaction picture for two spins can therefore be written

as [27]

$$\frac{\partial\hat{\rho}}{\partial t} = \iota[\hat{\rho},\hat{H}] + \sum_{i=1,2}\Big[\Gamma_i(t)\{n(\omega_i(t))+1\} \times\left(\hat{X}_i\hat{\rho}\hat{X}_i^\dagger - \frac{1}{2}\hat{X}_i^\dagger\hat{X}_i\hat{\rho} - \frac{1}{2}\hat{\rho}\hat{X}_i^\dagger\hat{X}_i\right) + \Gamma_i(t)n(\omega_i(t))\left(\hat{X}_i^\dagger\hat{\rho}\hat{X}_i - \frac{1}{2}\hat{X}_i\hat{X}_i^\dagger\hat{\rho} - \frac{1}{2}\hat{\rho}\hat{X}_i\hat{X}_i^\dagger\right)\Big], \tag{18}$$

where $\Gamma_i(t)\{n(\omega_i(t))+1\}$ and $\Gamma_i(t)n(\omega_i(t))$ are time-dependent dissipation rates, $n(\omega_i(t)) = [\exp(\frac{\hbar\omega_i(t)}{kT}) - 1]^{-1}$ is the average number of photons in the bath at the transition frequencies $\omega_i(t)$, $\Gamma_i(t) = 0.1\omega_i(t)e^{-\omega_i(t)/\omega_c}$ is the time-dependent dissipation rate of the spin to an Ohmic type bath [63,64], and ω_c is the cut-off frequency of the bath spectral density. These rates are time-dependent because of the timedependence of the Hamiltonian $\hat{H}(t)$ [63,65]. Note that we are assuming that Eq. (18) remains valid for the time scales involved with the system and the bath dynamics. This is possible if the bath time scale $1/\omega_c$ is much smaller than the system time-scale $1/\min_j(E_j)$ [where E_j is given by Eq. (3)] and the duration τ during which the magnetic field is changed [63].

Note that the jump operators associated to a system operator $\hat{X}$ are given by [66]

$$\hat{X}(\omega) = \sum_{\epsilon'-\epsilon=\omega} |\epsilon\rangle\langle\epsilon|\hat{X}|\epsilon'\rangle\langle\epsilon'|,$$

where $\{|\epsilon\rangle\}$ is the basis of the eigenvectors of the system Hamiltonian $\hat{H}$. In the present case, the first spin is assumed to interact with the heat bath via $\hat{\sigma}^x$ operator, and the corresponding jump operators $\hat{X}_i$ and the respective transition frequencies are given by

$$\hat{X}_1 = \frac{1}{2}\left(\frac{B+K-\gamma J}{\sqrt{K^2+BK}}|\psi_1\rangle\langle\psi_3| + \frac{B-K+\gamma J}{\sqrt{K^2-BK}}|\psi_0\rangle\langle\psi_2|\right), \quad \hbar\omega_1 = 2K+2J,$$
$$\hat{X}_2 = \frac{1}{2}\left(\frac{B+K+\gamma J}{\sqrt{K^2+BK}}|\psi_2\rangle\langle\psi_3| + \frac{B-K-\gamma J}{\sqrt{K^2-BK}}|\psi_0\rangle\langle\psi_1|\right), \quad \hbar\omega_2 = 2K-2J. \tag{19}$$

These operators satisfy the relations $[\hat{H},\hat{X}_i] = -\omega_i\hat{X}_i$ and $[\hat{H},\hat{X}_i^\dagger] = \omega_i\hat{X}_i^\dagger$. Note that K and $|\psi_{0,3}\rangle$ are functions of $B(t)$, and are therefore timedependent, which also gives rise to the time dependence of the jump operators in Eq. (19).

The heat and work in an open quantum system in the presence of an external drive are defined as [61]

$$Q(t) = \int_0^t \mathrm{Tr}[\dot{\hat{\rho}}(t')\hat{H}(t')]dt',$$
$$W(t) = \int_0^t \mathrm{Tr}[\hat{\rho}(t')\dot{\hat{H}}(t')]dt'. \tag{20}$$

The total change in the average energy of the system in a process is given by $\Delta E(t) = E(t) - E(0)$, where $E(t) = \mathrm{Tr}[\hat{\rho}(t)\hat{H}(t)]$ is the average energy at a time t. This change in energy can be written as contributions from two separate thermodynamic quantities as

$$\Delta E(t) = W(t) + Q(t). \tag{21}$$

The work in the AB and CD processes can then be represented as follows:

$$W_1(\tau) = \int_0^\tau \mathrm{Tr}[\hat{\rho}_{A\to B}(t')\dot{\hat{H}}_{A\to B}(t')]dt'$$
$$W_2(\tau) = \int_0^\tau \mathrm{Tr}[\hat{\rho}_{C\to D}(t')\dot{\hat{H}}_{C\to D}(t')]dt'. \tag{22}$$

So, the total work is given by $W = W_1 + W_2$. We calculated the heat transfer between the system and the heat bath using Eq. (21). The numerical solution of the master equation has been done using the fourthorder adaptive Runge-Kutta method and the numerical integration to calculate the work is done using the Trapezoidal rule. The heat absorption in the measurement process is calculated as discussed in Sec. II B.

We show in Fig. 6 how the efficiency varies with the duration τ of the unitary stages. It is clear from this plot that the presence of the bath has a negligible effect on its performance in a very short time. Therefore, we can employ such a measurement-based heat engine model whenever one requires a finite amount of power. One does not have to decouple the working system ever to obtain a finite amount of power, if the engine runs for a finite duration. However, the longer the duration τ, the more the engine efficiency decreases due to the dominant effects of the bath over the external control parameter. The dissipative part of the master equation dominates over the unitary part and therefore, the system releases more energy to the bath as heat than it releases as the work. Also, the spins absorb more energy during the measurement stage as τ increases. We must emphasize that if both the spins are

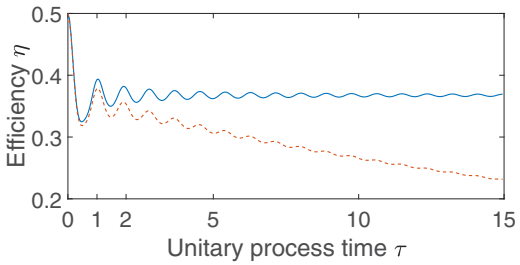

FIG. 6. Efficiency η as a function of duration τ of the unitary stages for $\Gamma_i(t) = 0$ (for the isolated system: solid blue line) and $\Gamma_i(t) = 0.1\omega_i(t)e^{-\omega_i(t)/\omega_c}$ (for open system: dashed red line). The other parameters are $B_1 = 1$, $B_2 = 2$, $T = 1$, $\omega_c = 1000$, and $\gamma = 1$.

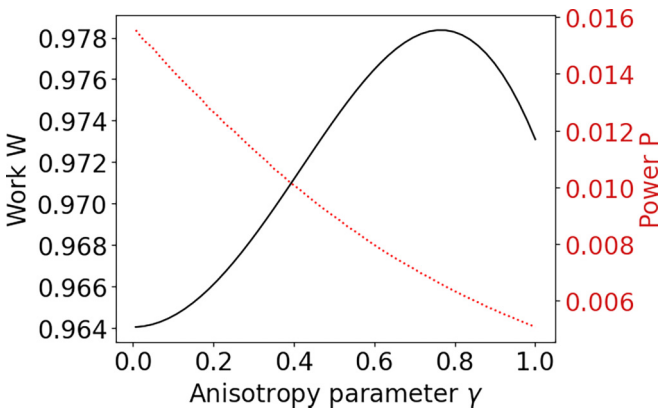

FIG. 7. Variation of the absolute value of work (black solid line, labeled on the left y axis) and power (point marked red line, labeled on the right y axis) as a function of the anisotropy parameter γ in the limit of $\tau \to 0$. A moderate thermalization time ranges from 61 to 191 for anisotropy $0 \leqslant \gamma \leqslant 1$ when the trace distance $D(\hat{\rho}, \hat{\rho}_A) \sim 10^{-2}$. The other parameters are $B_1 = 1, B_2 = 2, T = 1$.

considered to individually interact with the heat bath [67,68], the main results of this paper will remain the same.

In this section, we have considered the QOE with an always-on single bath along with a measurement protocol. On the other hand, it is possible for a QOE that operates with two heat baths to maintain such an always-on coupling, while still achieving a reciprocating cycle by periodically changing the interaction strength with the baths. However, as the performance of these QOEs deteriorates in a finite time, such an always-on interaction cannot give us operational advantages over a measurement-based engine.

A. Power analysis of the engine

The isochoric cooling process of the system with a thermal bath is not an instantaneous process, and ideally takes infinite time. To make a power analysis, we assume that the state of the system becomes very close to a thermal state ρ_A at a finite time t_c. In order to make an estimate of this closeness we have calculated the trace distance between two states $\hat{\rho}$ and $\hat{\rho}_A$, defined as $D(\hat{\rho}, \hat{\rho}_A) = \frac{1}{2}\,\mathrm{Tr}\,|\hat{\rho} - \hat{\rho}_A|$ [45], where the state $\hat{\rho}$ is obtained by solving the master equation [Eq. (18)], with time-independent dissipation rate coefficients, as the magnetic field is kept constant at $B = B_1$ during this cooling process. Also, as defined in Sec. II B, ρ_A represents the thermal state at a temperature T (that of the cold bath) when the magnetic field is maintained at $B = B_1$ [see also, Fig. (1)]. We estimated t_c, as a time when the trace distance $D(\hat{\rho}, \hat{\rho_A})$ becomes $\sim 10^{-2}$. Such a finite-time analysis of the cooling process helps us in defining the power of the engine as $P = W/(2\tau + t_c)$, where τ is the duration of each unitary stage, and we have assumed that the measurement is an instantaneous process. The plot of the power as a function of the anisotropy is shown in Fig. 7.

We found that in the limit of $\tau \to 0$, the work does not change substantially with respect to γ as compared to the quasistatic limit, which is discussed in Sec. III D. However, the thermalization time increases with the increase in anisotropy, leading to a reduction of power. Further, if we consider that both spins interact with the bath, thermalization of the system during the isochoric cooling process can be achieved at a much faster pace, and hence, more power would be generated by the engine.

V. CONCLUSIONS

We have studied the performance of a measurement-based QOE in a two-spin working system coupled by the Heisenberg anisotropic XY interaction. A nonselective quantum measurement is used to fuel the engine. The noncommuting nature of the Hamiltonian at two different times initiates transitions between the instantaneous energy eigenstates at finite time unitary processes. Furthermore, the instantaneous energy eigenstates do not coincide with the measurement basis states which causes some transition between them. The relevant thermodynamic quantities are calculated in terms of these transition probabilities. We found that the efficiency oscillates largely at short times when the two-spin system is coupled by an anisotropic interaction, while for isotropic interaction there is no oscillation. This oscillation in efficiency is explained in terms of interference between different transition probabilities at finite times. It is observed that the oscillation in efficiency dies out as the unitary processes extend for a longer time and eventually the efficiency approaches the quasistatic limit. Thus, proper control of the duration of unitary processes during transient times can lead to higher work output and less heat absorption. As a result, a finite-time engine can be more efficient than a quasistatic engine. The efficiency further increases with increasing anisotropy while in the quasistatic limit; it is observed that the performance deteriorates with an increase in anisotropy.

Also, we studied the performance of the HE under the condition of always-on coupling to the heat bath. We found that the presence of the bath has a negligible effect on its performance in a very short time limit. However, for a longer duration of the stages AB and CD, its performance degrades. This is primarily due to the dominance of the bath interaction over external control during these stages.

APPENDIX A: EIGENVECTORS AND EIGENVALUES FOR $\gamma = 0$ AND THE CORRESPONDING TRANSITION PROBABILITIES

In the limit of $\gamma \to 0$, the eigenstates and corresponding eigenvectors of the Hamiltonian $\hat{H}(t)$ take the following forms:

$$\begin{aligned} |\psi_0\rangle &= |00\rangle, & E_0 &= -2B, \\ |\psi_1\rangle &= \frac{1}{\sqrt{2}}(-|10\rangle + |01\rangle), & E_1 &= -2J, \\ |\psi_2\rangle &= \frac{1}{\sqrt{2}}(|10\rangle + |01\rangle), & E_2 &= 2J, \\ |\psi_3\rangle &= |11\rangle, & E_3 &= 2B. \end{aligned} \tag{A1}$$

Clearly, the states $|\psi_{0,3}\rangle$ are no longer entangled, though they differ from the Bell states $|\psi_\pm\rangle$. Also in this limit, it can be shown using the above eigenstates that the transition probabilities, as mentioned in Sec. III A, are reduced to $\delta = \lambda = \chi = 1/2$ and $\xi = 0$, where we used: $\langle\psi_0^{(2)}|\hat{U}(\tau)|\psi_3^{(1)}\rangle =$

$\langle\psi_3^{(2)}|\hat{U}(\tau)|\psi_0^{(1)}\rangle = \langle\psi_0^{(1)}|\hat{V}(\tau)|\psi_3^{(2)}\rangle = \langle\psi_3^{(1)}|\hat{V}(\tau)|\psi_0^{(2)}\rangle = 0$, and $\langle\psi_0^{(2)}|\hat{U}(\tau)|\psi_0^{(1)}\rangle = \langle\psi_3^{(1)}|\hat{V}(\tau)|\psi_3^{(2)}\rangle = 1$. Therefore, for the isotropic case, the efficiency becomes $\eta = 1 - B_1/B_2$, which does not depend on τ.

APPENDIX B: DERIVATION OF THE INTERNAL ENERGIES

1. At A: The Hamiltonian at point A of the cycle can be expressed as

$$\hat{H}_A = \hat{H}_1 = \sum_{i=0}^{3} E_i^{(1)} \big|\psi_i^{(1)}\big\rangle\big\langle\psi_i^{(1)}\big|,$$

where $\{|\psi_i^{(1)}\rangle\}$ are the eigenstates of the Hamiltonian $\hat{H}_1$. As we consider that the system at A is in thermal equilibrium with the heat bath, the thermal density matrix is given by

$$\hat{\rho}_A = \frac{e^{-\beta\hat{H}_1}}{Z} = \sum_{i=0}^{3} P_i \big|\psi_i^{(1)}\big\rangle\big\langle\psi_i^{(1)}\big|, \tag{B1}$$

where $P_i = e^{-\beta E_i^{(1)}}/Z$ is the thermal occupation probability of the ith eigenstate and Z is the relevant partition function. So, the average internal energy at point A is given by

$$\begin{aligned}\langle E_A\rangle &= \mathrm{Tr}(\hat{H}_1\hat{\rho}_A) = \sum_{i=0}^{3} P_i E_i^{(1)} \\ &= -4K_1\frac{\sinh 2K_1\beta}{Z} - 2J\frac{\sinh 2J\beta}{Z}.\end{aligned} \tag{B2}$$

2. At B: The Hamiltonian at point B of the cycle can be expressed as

$$\hat{H}_B = \hat{H}_2 = \sum_{i=0}^{3} E_i^{(2)} \big|\psi_i^{(2)}\big\rangle\big\langle\psi_i^{(2)}\big|,$$

where $\{|\psi_i^{(2)}\rangle\}$ are the eigenstates of the Hamiltonian $\hat{H}_2$. The density matrix at point B after the unitary process AB can be obtained as

$$\hat{\rho}_B = \hat{U}(\tau)\hat{\rho}_A\hat{U}^\dagger(\tau) = \sum_{i=0}^{3} P_i\hat{U}(\tau)\big|\psi_i^{(1)}\big\rangle\big\langle\psi_i^{(1)}\big|\hat{U}^\dagger(\tau). \tag{B3}$$

The average internal energy at the point B can be obtained as

$$\begin{aligned}\langle E_B\rangle &= \mathrm{Tr}(\hat{H}_2\hat{\rho}_B) \\ &= P_0E_0^{(2)}\big\langle\psi_0^{(2)}\big|\hat{U}(\tau)\big|\psi_0^{(1)}\big\rangle\big\langle\psi_0^{(1)}\big|\hat{U}^\dagger(\tau)\big|\psi_0^{(2)}\big\rangle \\ &\quad + P_3E_0^{(2)}\big\langle\psi_0^{(2)}\big|\hat{U}(\tau)\big|\psi_3^{(1)}\big\rangle\big\langle\psi_3^{(1)}\big|\hat{U}^\dagger(\tau)\big|\psi_0^{(2)}\big\rangle \\ &\quad + P_1E_1^{(2)} + P_2E_2^{(2)} + P_0E_3^{(2)}\big\langle\psi_3^{(2)}\big|\hat{U}(\tau)\big|\psi_0^{(1)}\big\rangle \\ &\quad \times\big\langle\psi_0^{(1)}\big|\hat{U}^\dagger(\tau)\big|\psi_3^{(2)}\big\rangle + P_3E_3^{(2)}\big\langle\psi_3^{(2)}\big|\hat{U}(\tau)\big|\psi_3^{(1)}\big\rangle \\ &\quad \times\big\langle\psi_3^{(1)}\big|\hat{U}^\dagger(\tau)\,\big|\psi_3^{(2)}\big\rangle \\ &= P_0E_0^{(2)}(1-\xi) + P_3E_0^{(2)}\xi + P_1E_1^{(2)} + P_2E_2^{(2)} \\ &\quad + P_0E_3^{(2)}\xi + P_3E_3^{(2)}(1-\xi) \\ &= -4K_2(1-2\xi)\frac{\sinh 2K_1\beta}{Z} - 4J\frac{\sinh 2J\beta}{Z},\end{aligned} \tag{B4}$$

where we have used the microreversibility conditions $|\langle\psi_0^{(2)}|\hat{U}(\tau)|\psi_3^{(1)}\rangle|^2 = |\langle\psi_3^{(2)}|\hat{U}(\tau)|\psi_0^{(1)}\rangle|^2 = \xi$ (proof is given in the Appendix C) and $|\langle\psi_0^{(2)}|\hat{U}(\tau)|\psi_0^{(1)}\rangle|^2 = |\langle\psi_3^{(2)}|\hat{U}(\tau)|\psi_3^{(1)}\rangle|^2 = 1-\xi$. In unitary stages for a short time interval τ, nonadiabatic transitions occur between energy eigenstates that are coupled [54]. In the present case, such transitions will be induced between the levels $|\psi_0\rangle$ and $|\psi_3\rangle$. So, the terms like $\langle\psi_0^{(2)}|\hat{U}(\tau)|\psi_1^{(1)}\rangle$, $\langle\psi_0^{(2)}|\hat{U}(\tau)|\psi_2^{(1)}\rangle$, and $\langle\psi_3^{(2)}|\hat{U}(\tau)|\psi_1^{(1)}\rangle$, etc., become zero.

3. At C: The density matrix after the measurement stage can be written as

$$\begin{aligned}\hat{\rho}_C &= \sum_{\alpha=1}^{4}\hat{M}_\alpha\hat{\rho}_B\hat{M}_\alpha = P_0\delta|\psi_+\rangle\langle\psi_+| + P_0(1-\delta)|\psi_-\rangle\langle\psi_-| \\ &\quad + P_1\big|\psi_1^{(1)}\big\rangle\big\langle\psi_1^{(1)}\big| + P_2\big|\psi_2^{(1)}\big\rangle\big\langle\psi_2^{(1)}\big| \\ &\quad + P_3(1-\delta)|\psi_+\rangle\langle\psi_+| + P_3\delta|\psi_-\rangle\langle\psi_-|,\end{aligned} \tag{B5}$$

where $\hat{M}_\alpha^\dagger = \hat{M}_\alpha$ and we have used the microreversibility condition $|\langle\psi_+|\hat{U}(\tau)|\psi_0^{(1)}\rangle|^2 = |\langle\psi_-|\hat{U}(\tau)|\psi_3^{(1)}\rangle|^2 = \delta$ (proof can be found in the Appendix C) and $|\langle\psi_-|\hat{U}(\tau)|\psi_0^{(1)}\rangle|^2 = |\langle\psi_+|\hat{U}(\tau)|\psi_3^{(1)}\rangle|^2 = 1-\delta$. The average internal energy at point C can be obtained as

$$\begin{aligned}\langle E_C\rangle &= \mathrm{Tr}(\hat{H}_2\hat{\rho}_C) \\ &= E_0^{(2)}P_0\delta\big|\big\langle\psi_0^{(2)}\big|\psi_+\big\rangle\big|^2 + E_0^{(2)}P_0(1-\delta)\big|\big\langle\psi_0^{(2)}\big|\psi_-\big\rangle\big|^2 \\ &\quad + E_0^{(2)}P_3(1-\delta)\big|\big\langle\psi_0^{(2)}\big|\psi_+\big\rangle\big|^2 + E_0^{(2)}P_3\delta\big|\big\langle\psi_0^{(2)}\big|\psi_-\big\rangle\big|^2 \\ &\quad + E_1^{(2)}P_1 + E_2^{(2)}P_2 + E_3^{(2)}P_0\delta\big|\big\langle\psi_3^{(2)}\big|\psi_+\big\rangle\big|^2 \\ &\quad + E_3^{(2)}P_3(1-\delta)\big|\big\langle\psi_3^{(2)}\big|\psi_-\big\rangle\big|^2 + E_3^{(2)}P_3(1-\delta) \\ &\quad \times\big|\big\langle\psi_3^{(2)}\big|\psi_+\big\rangle\big|^2 + E_3^{(2)}P_3\delta\big|\big\langle\psi_3^{(2)}\big|\psi_-\big\rangle\big|^2 \\ &= -4K_2(1-2\delta)(1-2\chi)\frac{\sinh 2K_1\beta}{Z} - 4J\frac{\sinh 2J\beta}{Z},\end{aligned} \tag{B6}$$

where we have used $|\langle\psi_0^{(2)}|\psi_+\rangle|^2 = |\langle\psi_3^{(2)}|\psi_-\rangle|^2 = \chi$ and $|\langle\psi_0^{(2)}|\psi_-\rangle|^2 = |\langle\psi_3^{(2)}|\psi_+\rangle|^2 = 1-\chi$, which can be proved using the conservation of probability:

$$\big|\big\langle\psi_0^{(2)}\big|\psi_-\big\rangle\big|^2 + \big|\big\langle\psi_3^{(2)}\big|\psi_-\big\rangle\big|^2 = 1.$$

4. At D: The density matrix at point D after the unitary process CD is given by

$$\hat{\rho}_D = \hat{V}(\tau)\hat{\rho}_C\hat{V}^\dagger(\tau). \tag{B7}$$

Similarly to points A, B, and C, we can derive the average internal energy at point D which is given by

$$\begin{aligned}\langle E_D\rangle &= \mathrm{Tr}(\hat{H}_1\hat{\rho}_D) = -4K_1(1-2\delta)(1-2\lambda)\frac{\sinh 2K_1\beta}{Z} \\ &\quad - 4J\frac{\sinh 2J\beta}{Z},\end{aligned} \tag{B8}$$

where we have used the microreversibility condition $|\langle\psi_0^{(1)}|\hat{V}(\tau)|\psi_+\rangle|^2 = |\langle\psi_3^{(1)}|\hat{V}(\tau)|\psi_-\rangle|^2 = \lambda$ (proof is

given in the Appendix C) and $|\langle\psi_3^{(1)}|\hat{V}(\tau)|\psi_+\rangle|^2 = |\langle\psi_0^{(1)}|\hat{V}(\tau)|\psi_-\rangle|^2 = 1-\lambda$.

APPENDIX C: PROOF OF THE MICROREVERSIBILITY CONDITIONS

We show below in details the proof of the relation $|\langle\psi_0^{(2)}|\hat{U}(\tau)|\psi_3^{(1)}\rangle|^2 = |\langle\psi_3^{(2)}|\hat{U}(\tau)|\psi_0^{(1)}\rangle|^2$:

$$\begin{aligned}\left|\left\langle\psi_3^{(2)}\middle|\hat{U}(\tau)\middle|\psi_0^{(1)}\right\rangle\right|^2 &= \left\langle\psi_3^{(2)}\middle|\hat{U}(\tau)\middle|\psi_0^{(1)}\right\rangle\left\langle\psi_0^{(1)}\middle|\hat{U}^\dagger(\tau)\middle|\psi_3^{(2)}\right\rangle \\ &= \left\langle\psi_3^{(2)}\middle|\hat{U}(\tau)\left(\mathbb{I} - \left|\psi_1^{(1)}\right\rangle\left\langle\psi_1^{(1)}\right| - \left|\psi_2^{(1)}\right\rangle\right.\right. \\ &\quad \left.\left.\times\left\langle\psi_2^{(1)}\right| - \left|\psi_3^{(1)}\right\rangle y\left\langle\psi_3^{(1)}\right|\right)\hat{U}^\dagger(\tau)\middle|\psi_3^{2}\right\rangle, \end{aligned} \tag{C1}$$

where we have used the completeness relation $\sum_{i=0}^{3}|\psi_i^{(1)}\rangle\langle\psi_i^{(1)}| = \mathbb{I}$. The above relation can then be rewritten as

$$\begin{aligned}&\left\langle\psi_3^{(2)}\middle|\hat{U}(\tau)\hat{U}^\dagger(\tau)\middle|\psi_3^{(2)}\right\rangle - \left|\left\langle\psi_3^{(2)}\middle|\hat{U}(\tau)\middle|\psi_3^{(1)}\right\rangle\right|^2 \\ &\quad = 1 - \left(1 - \left|\left\langle\psi_0^{(2)}\middle|\hat{U}(\tau)\middle|\psi_3^{(1)}\right\rangle\right|^2\right) \\ &\quad = \left|\left\langle\psi_0^{(2)}\middle|\hat{U}(\tau)\middle|\psi_3^{(1)}\right\rangle\right|^2. \end{aligned} \tag{C2}$$

In the last step of the above derivation, we have used the conservation of the probability:

$$\left|\left\langle\psi_0^{(2)}\middle|\hat{U}(\tau)\middle|\psi_3^{(1)}\right\rangle\right|^2 + \left|\left\langle\psi_3^{(2)}\middle|\hat{U}(\tau)\middle|\psi_3^{(1)}\right\rangle\right|^2 = 1.$$

Similarly, we can prove the other microreversibility conditions, namely, $|\langle\psi_+|\hat{U}(\tau)|\psi_0^{(1)}\rangle|^2 = |\langle\psi_-|\hat{U}(\tau)|\psi_3^{(1)}\rangle|^2$ and $|\langle\psi_0^{(1)}|\hat{V}(\tau)|\psi_+\rangle|^2 = |\langle\psi_3^{(1)}|\hat{V}(\tau)|\psi_-\rangle|^2$ by using $\sum_{\alpha=1}^{4}\hat{M}_\alpha^2 = \mathbb{1}$ and the conservation of probability, respectively,

$$\left|\left\langle\psi_+\middle|\hat{U}(\tau)\middle|\psi_3^{(1)}\right\rangle\right|^2 + \left|\left\langle\psi_-\middle|\hat{U}(\tau)\middle|\psi_3^{(1)}\right\rangle\right|^2 = 1,$$

$$\left|\left\langle\psi_0^{(1)}\middle|\hat{V}(\tau)\middle|\psi_-\right\rangle\right|^2 + \left|\left\langle\psi_3^{(1)}\middle|\hat{V}(\tau)\middle|\psi_-\right\rangle\right|^2 = 1.$$

[1] C. L. Latune, I. Sinayskiy, and F. Petruccione, Eur. Phys. J.: Spec. Top. **230**, 841 (2021).
[2] M. T. Mitchison, M. P. Woods, J. Prior, and M. Huber, New J. Phys. **17**, 115013 (2015).
[3] M. O. Scully, M. S. Zubairy, G. S. Agarwal, and H. Walther, Science **299**, 862 (2003).
[4] Y.-H. Shi, H.-L. Shi, X.-H. Wang, M.-L. Hu, S.-Y. Liu, W.-L. Yang, and H. Fan, J. Phys. A: Math. Theor. **53**, 085301 (2020).
[5] C. Latune, I. Sinayskiy, and F. Petruccione, Sci. Rep. **9**, 3191 (2019).
[6] K. Brandner, M. Bauer, M. T. Schmid, and U. Seifert, New J. Phys. **17**, 065006 (2015).
[7] R. Uzdin, A. Levy, and R. Kosloff, Phys. Rev. X **5**, 031044 (2015).
[8] R. Uzdin, Phys. Rev. Appl. **6**, 024004 (2016).
[9] K. Brandner, M. Bauer, and U. Seifert, Phys. Rev. Lett. **119**, 170602 (2017).
[10] M. O. Scully, K. R. Chapin, K. E. Dorfman, M. B. Kim, and A. Svidzinsky, Proc. Natl. Acad. Sci. USA **108**, 15097 (2011).
[11] S. Rahav, U. Harbola, and S. Mukamel, Phys. Rev. A **86**, 043843 (2012).
[12] N. Brunner, M. Huber, N. Linden, S. Popescu, R. Silva, and P. Skrzypczyk, Phys. Rev. E **89**, 032115 (2014).
[13] F. Altintas, A. U. C. Hardal, and O. E. Müstecaplıog˜lu, Phys. Rev. E **90**, 032102 (2014).
[14] G. A. Barrios, F. Albarrán-Arriagada, F. A. Cárdenas-López, G. Romero, and J. C. Retamal, Phys. Rev. A **96**, 052119 (2017).
[15] F. Altintas, A. Ü. C. Hardal, and Ö. E. Müstecaplıoğlu, Phys. Rev. A **91**, 023816 (2015).
[16] A. Hewgill, A. Ferraro, and G. De Chiara, Phys. Rev. A **98**, 042102 (2018).
[17] T. Zhang, W.-T. Liu, P.-X. Chen, and C.-Z. Li, Phys. Rev. A **75**, 062102 (2007).
[18] A. Das and S. Ghosh, Entropy **21**, 1131 (2019).
[19] G. Thomas and R. S. Johal, Phys. Rev. E **83**, 031135 (2011).
[20] S. Çakmak, F. Altintas, and Ö. E Müstecaplıoğlu, Eur. Phys. J. Plus **131**, 197 (2016).
[21] S. Çakmak, D. Türkpençe, and F. Altintas, Eur. Phys. J. Plus **132**, 554 (2017).
[22] F. Altintas and Ö. E. Müstecaplıoğlu, Phys. Rev. E **92**, 022142 (2015).
[23] E. A. Ivanchenko, Phys. Rev. E **92**, 032124 (2015).
[24] X. L. Huang, A. N. Yang, H. W. Zhang, S. Q. Zhao, and S. L. Wu, Quantum Inf. Proc. **19**, 242 (2020).
[25] X. Huang, Y. Liu, Z. Wang, and X. Niu, Eur. Phys. J. Plus **129**, 4 (2014).
[26] G. De Chiara and M. Antezza, Phys. Rev. Res. **2**, 033315 (2020).
[27] X. L. Huang, T. Wang, X. X. Yi *et al.*, Phys. Rev. E **86**, 051105 (2012).
[28] J. Roßnagel, O. Abah, F. Schmidt-Kaler, K. Singer, and E. Lutz, Phys. Rev. Lett. **112**, 030602 (2014).
[29] R. Alicki and D. Gelbwaser-Klimovsky, New J. Phys. **17**, 115012 (2015).
[30] R. J. de Assis, T. M. de Mendonça, C. J. Villas-Boas, A. M. de Souza, R. S. Sarthour, I. S. Oliveira, and N. G. de Almeida, Phys. Rev. Lett. **122**, 240602 (2019).
[31] M. O. Scully, Phys. Rev. Lett. **87**, 220601 (2001).
[32] J. Klaers, S. Faelt, A. Imamoglu, and E. Togan, Phys. Rev. X **7**, 031044 (2017).
[33] W. Niedenzu, V. Mukherjee, A. Ghosh, A. G. Kofman, and G. Kurizki, Nat. Commun. **9**, 165 (2018).
[34] K. Maruyama, F. Nori, and V. Vedral, Rev. Mod. Phys. **81**, 1 (2009).
[35] H. Li, J. Zou, J.-G. Li, B. Shao, and L.-A. Wu, Ann. Phys. **327**, 2955 (2012).
[36] A. N. Jordan, C. Elouard, and A. Auffèves, Quantum Stud. Math. Found. **7**, 203 (2020).
[37] S. Chand and A. Biswas, Europhys. Lett. **118**, 60003 (2017).
[38] S. Chand and A. Biswas, Phys. Rev. E **95**, 032111 (2017).

[39] S. Chand, S. Dasgupta, and A. Biswas, Phys. Rev. E **103**, 032144 (2021).
[40] J. Yi, P. Talkner, and Y. W. Kim, Phys. Rev. E **96**, 022108 (2017).
[41] T. Denzler and E. Lutz, Phys. Rev. Res. **2**, 032062 (2020).
[42] R. Dann, R. Kosloff, and P. Salamon, Entropy **22**, 1255 (2020).
[43] Y. Rezek and R. Kosloff, New J. Phys. **8**, 83 (2006).
[44] S. Lee, M. Ha, J.-M. Park, and H. Jeong, Phys. Rev. E **101**, 022127 (2020).
[45] P. A. Camati, J. F. G. Santos, and R. M. Serra, Phys. Rev. A **99**, 062103 (2019).
[46] S. Çakmak, F. Altintas, A. Gençten, and Ö. E. Müstecaplıoğlu, Eur. Phys. J. D **71**, 1 (2017).
[47] D. Türkpençe and F. Altintas, Quant. Info. Proc. **18**, 1 (2019).
[48] B. Çakmak and Ö. E. Müstecaplıoğlu, Phys. Rev. E **99**, 032108 (2019).
[49] F. Plastina, A. Alecce, T. J. G. Apollaro, G. Falcone, G. Francica, F. Galve, N. Lo Gullo, and R. Zambrini, Phys. Rev. Lett. **113**, 260601 (2014).
[50] Y. Rezek, Entropy **12**, 1885 (2010).
[51] A. Dodonov, D. Valente, and T. Werlang, J. Phys. A: Math. Theor. **51**, 365302 (2018).
[52] P. Abiuso and V. Giovannetti, Phys. Rev. A **99**, 052106 (2019).
[53] Z. Lin, S. Su, J. Chen, J. Chen, and J. F. G. Santos, Phys. Rev. A **104**, 062210 (2021).
[54] C. Cherubim, T. R. de Oliveira, and D. Jonathan, Phys. Rev. E **105**, 044120 (2022).
[55] S. Suzuki, J.-I. Inoue, and B. K. Chakrabarti, *Quantum Ising Phases and Transitions in Transverse Ising Models*, Lecture Notes in Physics Vol. 862 (Springer, Berlin, Heidelberg, 2013).
[56] G. L. Kamta and A. F. Starace, Phys. Rev. Lett. **88**, 107901 (2002).
[57] Y. Yeo, T. Liu, Y.-E. Lu, and Q.-Z. Yang, J. Phys. A: Math. Gen. **38**, 3235 (2005).
[58] J. R. Johansson, P. D. Nation, and F. Nori, Comput. Phys. Commun. **183**, 1760 (2012).
[59] G. Jiao, S. Zhu, J. He, Y. Ma, and J. Wang, Phys. Rev. E **103**, 032130 (2021).
[60] N. Piccione, G. De Chiara, and B. Bellomo, Phys. Rev. A **103**, 032211 (2021).
[61] G. Kurizki and A. G. Kofman, *Thermodynamics and Control of Open Quantum Systems* (Cambridge University Press, Cambridge, UK, 2022).
[62] S. Bhattacharjee and A. Dutta, Eur. Phys. J. B **94**, 239 (2021).
[63] R. Dann, A. Levy, and R. Kosloff, Phys. Rev. A **98**, 052129 (2018).
[64] A. J. Leggett, S. Chakravarty, A. T. Dorsey, M. P. Fisher, A. Garg, and W. Zwerger, Rev. Mod. Phys. **59**, 1 (1987).
[65] T. Albash, S. Boixo, D. A. Lidar, and P. Zanardi, New J. Phys. **14**, 123016 (2012).
[66] H.-P. Breuer, F. Petruccione *et al.*, *The Theory of Open Quantum Systems* (Oxford University Press on Demand, 2002).
[67] L.-Z. Hu, Z.-X. Man, and Y.-J. Xia, Quantum. Inf. Proc. **17**, 1 (2018).
[68] J.-Q. Liao, J.-F. Huang, L.-M. Kuang *et al.*, Phys. Rev. A **83**, 052110 (2011).